Contents lists available at ScienceDirect

Soil Dynamics and Earthquake Engineering

Site characterization at Chilean strong-motion stations: Comparison of downhole and microtremor shear-wave velocity methods

Sheri Molnar [a,*], Carlos E. Ventura [a], Ruben Boroschek [b], Manuel Archila [a]

[a] University of British Columbia, Earthquake Engineering Research Facility, 2235 East Mall, Vancouver, BC, Canada V6T 1Z4
[b] University of Chile, Department of Civil Engineering, Beauchef 850, Santiago, Chile

ARTICLE INFO

ABSTRACT

A blind comparison of independent invasive (downhole, standard penetration, bender element) and non-invasive microtremor shear-wave velocity (V_S) profiling is presented for 11 strong-motion stations in central and southern Chile that recorded the 2010 M_W 8.8 Maule earthquake. For the majority of stations, site classification based on average V_S in the upper 30 m (V_{S30}) is consistent irrespective of methodology. For a variety of geological conditions, excellent to good agreement is obtained between invasive and non-invasive V_S structure at five stations over the entire borehole length and in the uppermost layer at three stations. Site classification based on site period is evaluated using earthquake and microtremor recordings. Short site periods are observed at stiff coarse-grained stations whereas longer site periods are observed at soft fine-grained stations. The use of both V_{S30} and site period criteria are recommended in future revisions of the Chilean building code for robust earthquake site response characterization.

1. Introduction

Earthquake ground shaking is amplified by the presence of material with reduced shear-wave velocity (V_S) generally towards surface. Currently, most building codes classify site conditions for seismic site response based on average properties of the upper 30-m such as the travel-time averaged shear-wave velocity (V_{S30}), average standard penetration resistance (N_{60}), and soil undrained shear strength (S_u). The Chilean building code [1 and references therein] adopted the use of V_{S30} as the main parameter for seismic site classification (Table 1) primarily due to observed damage in deep sandy deposits in downtown Concepcion following the 2010 M_W 8.8 Maule, Chile, subduction earthquake.

A variety of invasive and non-invasive field methodologies have been developed to provide a reliable V_S-depth profile at a site, for which the least expensive and time-consuming method is of particular interest. Invasive testing methods provide detailed, but restricted, information of the subsurface within the tested soil column with cost directly related to penetration depth. Non-invasive surface seismic methods provide broad-stroke subsurface imaging without direct retrieval of small-scale structure or geologic material for lower cost and less site disruption. In reality, combinations of invasive and non-invasive V_S profiling methods are generally used together for earthquake site response assessment, due to their inherent advantages and disadvantages.

Non-invasive surface-wave methods may be further categorized by the use of an active source, e.g. hammer impact, or a passive source, e.g. ambient vibrations. Active-source surface-wave seismic techniques, such as spectral analysis, SASW [2], or multichannel analysis, MASW [3], of surface waves, generally offer a restricted investigation depth (a few tens of meters) related to the frequency content of the source. The microtremor array method [4–6], a passive-source method that uses background ambient vibrations with a wide frequency content from a variety of natural and man-made sources, is generally sensitive to greater depth, e.g. ≥ 100 m [6,7]. It is important to note that measured field data of discrete invasive V_S measurements and surface-wave dispersion data are not directly comparable: the discrete V_S measurements must be converted to a continuous V_S-depth function in order to compare with either the inverted continuous V_S-depth function of the surface-wave dispersion data or converted to dispersion estimates for comparison with the measured dispersion data.

Independent evaluations of non-invasive surface wave methods with respect to well-regarded invasive methods, i.e. blind test

Table 1
Site classification based on V_{S30} in revised Chilean building code [1].

Site class	Description	V_{S30} range (m/s)
A	Rocks, cemented soils	≥ 900
B	Soft or fractured rocks, very dense or very firm soils	≥ 500
C	Dense or firm soils	≥ 350
D	Medium dense or medium firm soils	≥ 180
E	Medium loose soils	< 180
F	Special soils	

comparison, were accomplished in the 1990s during development of the non-invasive methods. For example, at Fraser River delta sites, south of Vancouver, Canada, the average relative difference in V_S to a maximum 30-m depth between the optimal inversion result of active-source (MASW or SASW) acquired dispersion data and invasive (downhole or SCPT) V_S measurements is 25% or better [8–10]. Blind-test comparison of the Bayesian inversion result of microtremor-array acquired dispersion data and invasive downhole and SCPT V_S measurements resulted in an average relative difference in V_S of 5% to 120-m depth [7] and 25% to 60-m depth [11]. Otherwise few case studies of blind-test comparisons are available at sites that have experienced strong earthquake shaking; when discrete invasive-method V_S measurements are available they are generally used to constrain the inversion of non-invasive dispersion data for V_S-depth structure (profiles). A comprehensive examination of 9 blind-test comparisons of invasive and non-invasive V_S profiling methods at sites in California determined that for V_{S30} estimates > 200 m/s, invasive-method estimates are biased higher than non-invasive method estimates [12]; the coefficient-of-variation of V_{S30} estimates was determined to be 1–3% for co-located invasive methods, 5–6% for co-located non-invasive SASW methods, and 20–35% for correlated V_{S30} estimates per geologic unit. Variability in V_{S30} estimates becomes a significant issue when the estimates span the boundary between site classifications.

Subsurface soil properties beneath Chilean strong-motion stations were relatively unknown until recently [13]. The central part of Chile has been subjected to notable periodicity of large $M_W \geq 7.8$ earthquakes, with an average (one standard deviation) recurrence interval of 82 (6) years [14] due to rapid convergence of the oceanic Nazca plate beneath the continental South America plate. Prior to the 2010 M_W 8.8 Maule earthquake, no site-specific subsurface information was available for Chilean strong-motion stations outside of Santiago. As such, the University of Chile (UCH) Research and Material Testing Institute (Instituto de Investigación y Ensayo de Materiales, IDIEM) Civil Engineering Department (Departamento de Ingeniería Civil, DIC) conducted an invasive borehole testing campaign at 11 strong-motion stations in central and southern Chile (Fig. 1) following the M_W 8.8 Maule earthquake. The UCH–IDIEM–DIC invasive testing campaign provides a detailed comprehensive assessment of the subsurface column of drilled material at each strong-motion station. Conversely, the University of British Columbia (UBC) Earthquake Engineering Research Facility (EERF) of Vancouver, British Columbia, Canada, performed a rather crude non-invasive field testing campaign at these same 11 Chilean strong-motion stations. The UBC-EERF campaign was optimized for efficiency and budget by minimization of equipment, personnel, and time; however, a state-of-the-art probabilistic (Bayesian) inversion technique [7] is used to resolve subsurface V_S structure from the non-invasive dispersion data.

Rather than measure shear-wave velocity to classify subsurface ground conditions to predict site response, measured earthquake site response itself may be used to classify site conditions at
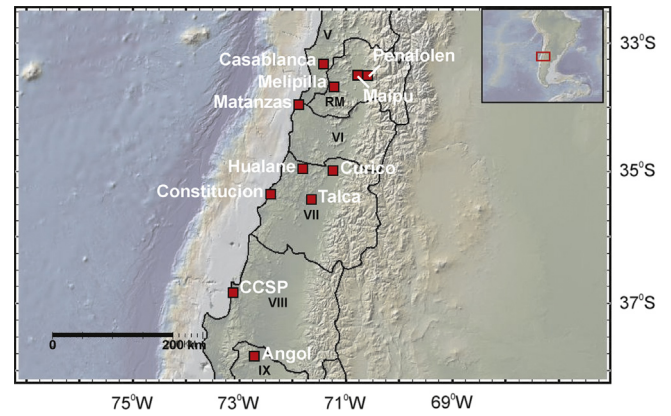
Fig. 1. Locations of 11 investigated Chilean strong-motion stations (squares) with regional districts (V–IX) marked by solid lines.

Table 2
Site classification based on site period [25].

Site class	Description	Natural period range
I	Rock/Stiff soil	$T < 0.2$ s
II	Hard soil	0.2 s $\leq T < 0.4$ s
III	Medium soil	0.4 s $\leq T < 0.6$ s
IV	Soft soil	$T \geq 0.6$ s
V	Generic rock	Flat H/V, T not identifiable.
VI	Generic soft soil	Broad amplification/multiple peaks above 0.2 s
VII	Unclassifiable	Multiple peaks over 0.2 s, T not identifiable.

strong-motion stations. Empirical earthquake site response is ideally determined from a multitude of weak to strong earthquake recordings at a variety of azimuths via standard bedrock-reference [15] and/or single instrument horizontal-to-vertical (H/V) [16] spectral ratios. The empirical spectral ratio is a measure of the amplification spectra (transfer function) resulting from the site-specific subsurface ground conditions. Microtremor H/V ratios have been shown to reliably measure predominant site period in comparison with weak to strong earthquake recordings e.g., [14,17–19]. Site classification based on the predominant period of the average H/V ratio has been proposed for strong-motion stations in Iran [20,21], Taiwan [22], Japan [23,24], and Italy [25]. Table 2 lists seven proposed period-based site classifications [25]; a short site period corresponds to rock or stiff soils, whereas a long site period corresponds to soft soils. Generic rock or soil classifications are proposed in the case of no predominant period or multiple peaks, respectively. For the 11 Chilean strong-motion stations, available earthquake recordings, as well as the non-invasive microtremor recordings, provide additional and unique datasets to evaluate site classification based on predominant site period.

This paper presents a blind comparison of the subsurface V_S-depth structure determined via invasive and non-invasive microtremor array method techniques at 11 strong-motion stations in central and southern Chile that recorded strong ground shaking from the 2010 M_W 8.8 Maule earthquake. The invasive testing results [26] were not made available to the first author until the microtremor data were processed and inverted for V_S structure, i.e. a blind test. The comparison of invasive and non-invasive V_S-profiling methods is performed in terms of the average relative difference in V_S for particular depth ranges and the resulting site classification based on V_{S30}. The non-invasive microtremor recordings, in combination with available earthquake recordings at the 11 Chilean strong-motion stations, allows for a

Table 3
Details of 11 investigated strong-motion stations in central and southern Chile.

Station code – city (region), location	Coords. (°S, °W)	Invasive method		Non-invasive method		Earthquake PGA	
		Borehole depth (m)	Borehole geology (thickness, m)	Array spacing	Min., Max. depth (m)[a]	M_W 8.8 event (g)[b]	M_S 7.8 event (g)[c]
CSCH – Casablanca (V), Teatro Municipal	33.32, 71.41	50	Alternating silt and sand (46.2 m) over gravel.	5, 15 m	14, 65	0.33	
CRS – Santiago Maipu (RM), Hospital	33.50, 70.77	30.45	Gravel (8.5 m) over silty sand (pumicite).	5, 15 m	7, 22	0.56	
HSOR-Santiago Penalolen (RM), Hospital Santiago Oriente	33.50, 70.58	31	Alternating silt, clay, and gravel (31 m).	5, 15 m	14, 80	0.30	
MELP – Melipilla (RM), Compania de Bomberos	33.69, 71.21	60	Sands and clays (6 m) over gravel (53.5 m) over conglomerate.	15, 30 m Same block	8, 47	0.78	0.67
MAT – Matanzas (VI), Escuela Carlos Ibanez del Campo	33.96, 71.87	50	Alternating sand and clay (50 m).	5, 15 m	8, 38	0.34	
HUA – Hualane (VII), Hospital	34.95, 71.80	61.45	Alternating clay, sand, and gravel (23.5 m) over alternating conglomerate and argillite.	6.4 m	20, 40	0.46	0.17
CUR – Curico (VII), Hospital	34.98, 71.24	15	Silty sand (10 m) over sandy gravel.	5, 11 m Across street	5, 27	0.47	0.18[d] 0.14[e]
CON – Constitucion (VII), Hospital	35.34, 72.41	50.4	Silts, clays, and sands (22. 5 m) over sandstone (18 m), conglomerate (6.5 m) and argillite.	5, 15 m	5, 60	0.64	0.14
TAL – Talca (VII), Colegio San Pio X	35.43, 71.63	60	Gravel (15 m) over alternating volcanic tuff, clay, and gravel.	5, 15 m	5, 60	0.48	0.17
CCSP – Concepcion (VIII), Colegio San Pedro de la Paz	36.84, 73.11	80.75	Silty sand (4.5 m) and clay (21 m) over fractured metamorphic rock.	5, 15 m	5, 50	0.65	
ANGO – Angol (IX), Hospital	37.80, 72.71	50	Clay and silty sand (13.5 m) over gravel (3.5 m) over alternating volcanic tuff, breccia, and bouldery gravel.	5, 15 m	4, 28	0.93	

[a] depth $= 1/2*(V_R/f)$.
[b] Max. PGA as reported in [26] and [48].
[c] Max. PGA as reported in [49].
[d] 28.02.2010 M6.6 earthquake.
[e] 28.08.2004 M_W 6.4 earthquake.

second and independent evaluation of site classification based on predominant site period.

2. Geological setting and microtremor microzonation studies

Relevant information regarding the site conditions at the investigated strong-motion stations, such as geological setting and V_S measurements, are described from north to south here. Generally, stations on the outer western coastline occur on Miocene marine sedimentary terraces atop the coastal batholith of Late Paleozoic igneous rocks, whereas stations eastward in the down-warped Central Depression overlie Mesozoic to Quaternary alluvial deposits derived from the Andean Cordillera to the east [27]. Volcanic pyroclastic tuff from the Maipo Caldera ($\sim 34°$S) is widely distributed over most of the Central Depression, including the Santiago basin, and was channeled westward along the main river valleys to the coast.

In Casablanca, alluvial fill of the Casablanca basin is composed largely of intercalated lenses of unconsolidated clay and sand with relatively little gravel, which overlies intrusive igneous rocks such as diorite and/or granodiorite [28]. The axis of deepest fill is on the south side of the valley and reaches a known maximum thickness of 54 m. Maipu and Penalolen occur in the southwest and east central metropolitan area of Santiago, respectively. The Santiago basin is primarily composed of colluvial pebbles and gravels in the east at Penalolen and clays and volcanic ash in the west at Maipu [29]. Seismic refraction studies indicate V_S of the upper 20-m of Santiago gravels range in V_S from 480-720 m/s and overlie ≥ 1300 m/s rock [30,31]. V_S in the upper 20-m of Santiago clays and volcanic ash is 120–350 m/s and 180–450 m/s, respectively [31]. In Constitucion, substantial tsunami inundation and vertical subsidence of the city occurred following the M_W 8.8 Maule earthquake; however, the strong-motion station was not inundated as the hospital is situated at the base of surrounding hills. At 8 sites in Constitucion, the average (one standard deviation) in V_S of the upper 6 m is 199 (52) m/s [32]. The city of Curico is composed of alluvial deposits of the Teno River, with coarse-grained gravels in the proximal eastern deposits and progressively finer-grained sands and silts in the western distal deposits, which is disrupted by the presence of fine-grained sand banks of inactive fluvial-channel and lacustrine deposits [33]. Active fluvial terraces and channels occur towards the south. The strong-motion station in Talca occurs in a transition zone of complex interbedding between Maule alluvial sediments of the southwest and volcanic ashes, lapilli, and pumice of the north [33]. The average (one standard deviation) V_S of the upper 6 m at 13 sites is 314 (135) m/s [32]. The Concepcion San Pedro de la Paz (CCSP) strong-motion station is located on the peninsula across the Bio Bio river from downtown Concepcion. Surficial black basaltic sands are carried by the Bio Bio river from the Andes [34]; gravels exhibit V_S of 850 m/s [32]. Northeast of the strong-motion station, significant instances of liquefaction and lateral spreading were observed in the Bayona neighborhood, as well as uplift and tilting of underground sewage tanks, due to the M_W 8.8 earthquake shaking [34].

In Chile, microtremor measurements have been performed primarily at strong-motion stations in the Santiago metropolitan area for validation with earthquake recordings [35–38], but also for earthquake site effect assessment in Santiago [29,30,39], Concepcion [40], and Llolleo [14]. Overall, these studies demonstrated similar fundamental peak periods of the average horizontal-to-vertical (H/V) spectral ratio using both microtremor and weak to strong earthquake recordings (and in lieu of recordings, correlation with observed earthquake intensities from the 1985 M_S 7.8 Valparaiso and M_W 8.8 Maule earthquakes) suggesting that use of single-instrument microtremor recordings for site effect

assessment at locations in central and southern Chile is valid. However, microtremor H/V curves generally do not provide short-period (< 0.2 s) peaks as observed in earthquake H/V curves, which are related to shallow soils and correlate with damage of low-rise buildings [29,39]. The agreement in peak period at Santiago strong-motion stations from both microtremor and strong earthquake recordings is likely due to the rather stiff soils beneath Santiago. Potential non-linear response was demonstrated at strong-motion stations in Valparaiso and Vina del Mar [41], marked by a shift to longer peak period for stronger M_S 7.8 main-shock recordings compared to weaker aftershock recordings.

Following the M_W 8.8 Maule earthquake, several microtremor surveys were performed repeatedly by various research groups at strong-motion stations and/or locations of observed damage (potential site effect) in central Chile [33,41–44]. From examination of microtremor H/V results at over 700 locations in Talca and Curico [33], areas characterized by flat H/V curves are correlated with lower observed intensities and the presence of coarse-grained materials, whereas locations characterized by clear peaks are correlated with the higher intensities and the presence of fine-grained materials. Similarly, microtremor results at over 250 locations across Santiago [29] demonstrates clear H/V peaks are correlated with low (< 350 m/s) V_S surficial material, flat H/V curves or low-amplitude H/V peaks are correlated with the Santiago and Mapocho gravels, and broad H/V curves are correlated with rapidly varying sub/surface topography.

3. Site classification based on V_{S30}

Two types of V_S profiling are accomplished at the 11 Chilean strong-motion stations. First, discrete invasive downhole V_S measurements are accomplished along the length of each station's borehole by UCH–IDIEM–DIC. Non-invasive passive-source microtremor array testing is performed by UBC-EERF at each drilled borehole location to obtain dispersion data for probabilistic inversion of V_S profiles. Table 3 provides details of the invasive and non-invasive testing campaigns for the 11 investigated stations.

3.1. Invasive V_S profiling

Within each borehole, UCH–IDIEM–DIC documented water table depth and stratigraphy and performed downhole compression-wave velocity (V_P), V_S, and standard penetration test (SPT) measurements [26]. SPT measurements were not conducted at Talca due to very stiff geological conditions. Further laboratory testing of extracted borehole material samples included soil classification, bender element (BE) V_S testing, and unconfined compression tests. Laboratory BE V_S tests were performed using air-dried 45-cm samples at depth-dependent confining pressures. For Curico, the UCH–IDIEM–DIC report provides SPT and downhole V_P and V_S measurements (averaged per stratigraphic horizon) accomplished in 2003 to 15-m depth. For the other 10 stations, the average duration of water level monitoring and laboratory material testing is ~ 11 days each per location. Downhole V_P and V_S measurements are conducted within a single day per location over the course of 3 months. Overall, the detailed and comprehensive UCH–IDIEM–DIC invasive testing program occurred over a period of ~ 6 months.

For this study, SPT N (blowcount) values were converted to V_S using an average of 8 and 6 relations for sand and clay, respectively (Table 4). Sand or clay relations were chosen based on soil classifications in the UCH–IDIEM–DIC geotechnical report. Fig. 2 presents the discrete downhole, laboratory BE, and converted SPT V_S data in relation to the documented stratigraphic layering for the 11 investigated stations. Table 3 provides summarized geologic stratigraphy

Table 4
SPT blowcount (N) to V_S relations for sand and clay sediments[a].

Sand	Clay	Reference
$31.7N^{0.54}$		Shibata (1970)
$87.2N^{0.36}$		Ohta et al. (1972)
$80.6N^{0.331}$	$80.2N^{0.292}$	Imai (1977)
$100.5N^{0.29}$		Sykora and Stokoe (1983)
$125N^{0.3}$		Okamoto et al. (1989)
$57.4N^{0.49}$	$114.43N^{0.31}$	Lee (1990)
	$76.55N^{0.445}$	Athanasopoulos (1995)
	$27N^{0.73}$	Jafari et al. (2002)
$90.82N^{0.319}$	$97.89N^{0.269}$	Hasancebi and Ulusay (2006)
$73N^{0.33}$	$44N^{0.48}$	Dikmen (2009)

[a] Selected from Table 1.1 of [50], references therein.

of each borehole. For SPT N values reported as refusal, a default V_S of 500 m/s is used for plotting. The BE V_S values tend to agree with the downhole V_S data overall, but in some instances, varies significantly. The converted SPT N values are similar to the downhole V_S measurements overall, except over particular depth ranges at Casablanca and Penalolen. At Penalolen, the soil classification is primarily clay and the conversion to V_S values is similar to the downhole V_S data only in the near-surface. It is worth noting that geological horizons are not always accompanied by a shift in V_S.

For an initial assessment of V_{S30}, the discrete invasive-methods V_S measurements, primarily downhole, as well as laboratory BE and converted SPT V_S values, are converted to a V_S depth profile. The mean invasive-methods V_S is calculated based on V_S values within selected depth intervals (layering) based first on V_S
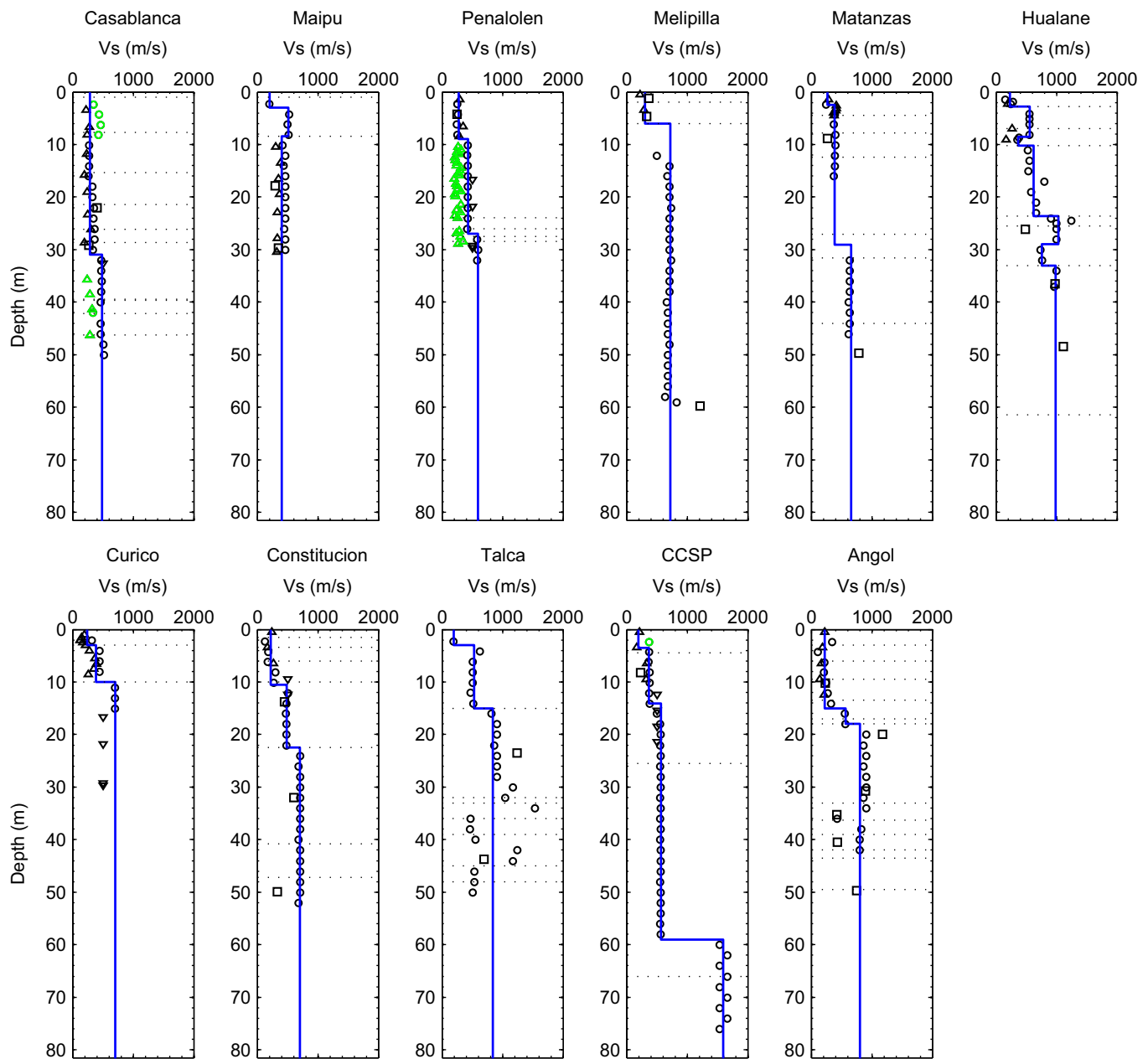
Fig. 2. Invasive method V_S measurements for the 11 investigated borehole locations: downhole (circles), laboratory BE (squares), and converted SPT (upward triangle). SPT refusal measurements (downward triangle) are set to 500 m/s and stratigraphic horizons denoted by dotted lines. The mean invasive-methods V_S profile is denoted by the solid line; V_S measurements not used in the averaging shown in a lighter color.

Table 5
Assessment of V_{S30}.

Strong-motion station	Microtremor dispersion (V_{R40}) data		V_S profiling methods				Other published studies	
			Inverted V_S models[c]		Average invasive-methods V_S profile[d]			
	V_{S30}[a]	Class[b]	V_{S30} (std. dev.)	Class[b]	V_{S30}	Class[b]	V_{S30}	Class[b]
Casablanca	303	D	306 (20)	100% D	290	D		
Maipu	439	C	N/A	–	386	C	392 [42]	C
Penalolen	303	D	330 (15)	100% D	379	C	408 [42]	C
Melipilla	N/A	–	750 (67)	100% B	566	B	724 [13]	B
Matanzas	334	D	374 (33)	76% C 24% D	374	C		
Hualane	460	C	N/A	–	547	B	523 [42] 527 [13]	B
Curico	533	B	554 (80)	62% B 38% C	592-710	B	564 [42]	B
Constitucion	261	D	264 (25)	100% D	360	C	230 [42] 595 [13]	D B
Talca	606	B	677 (21)	100% B	537–606	B	585 [42]	B
CCSP	N/A	–	271 (7)	100% D	398	C		
Angol	~376	C	372 (50)	62% C 36% D	348	D		

[a] Calculated using relation of [47].
[b] Defined in Table 1.
[c] Inverted V_S profiles of Fig. 6.
[d] Mean invasive-methods V_S profile shown in Figs. 2 and 7.
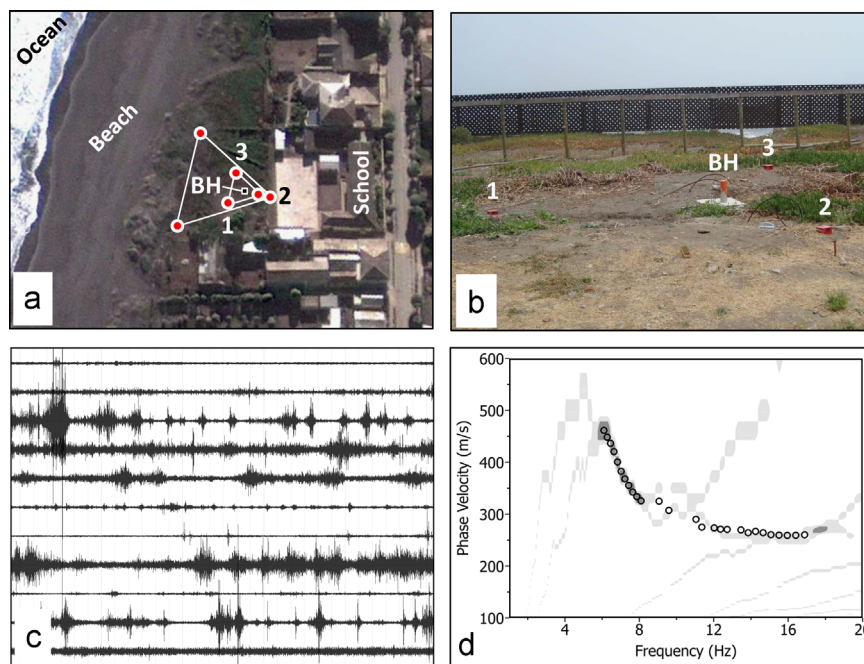
Fig. 3. (a) Overview map of 5-m and 15-m equilateral triangular arrays at Matanzas. Each sensor is numbered and marked by a circle and the borehole (BH) location is marked by a square. (b) Photo of 5-m array at Matanzas. (c) Example 5-min duration microtremor recordings at all 11 sites. (d) MSPAC dispersion histogram for Matanzas. Final phase velocity estimates extracted for inversion are shown as open circles.

variation with secondary consideration to geological strata variation. Table 5 lists the V_{S30} estimate based on the mean invasive-methods V_S-depth profile determined here for each station and associating site class based on the current Chilean building code requirement [1 and references therein]. Overall, stations with coarse-grained material (gravel) within the upper 10-m correspond to class B (soft or fractured rocks, very dense or very firm soils) or C (dense or firm soils): Curico, Hualane, Maipu, Melipilla, and Talca. All other stations are comprised of finer-grained sands and clays and correspond to class D (firm to medium firm soil conditions).

3.2. Non-invasive V_S profiling

At each borehole location in Chile, simultaneous microtremor array measurements were collected by the first and fourth authors using 3 TROMINO® sensors spaced equidistantly in a triangular configuration, usually at 5 and 15 m (Fig. 3 and Table 3). Equipment was kept to a minimum for ease of transport in aircraft and vehicles. Time spent in the field was also minimized to 2 array setups of 30 min duration per location, in order to accomplish measurements at all 11 stations, spanning 1100 km, within 10 days. Transportation and logistics were provided locally by UCH–
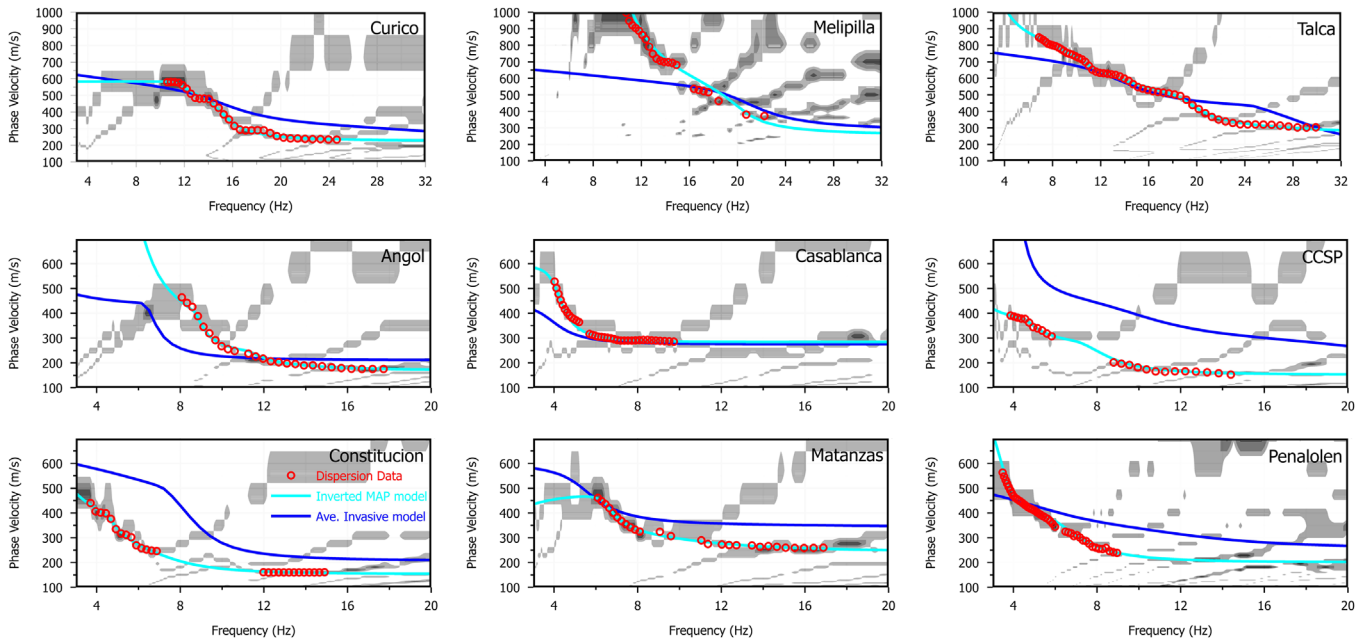
Fig. 4. Final phase velocity estimates (open circles) determined for 9 investigated strong-motion stations from microtremor array data (MSPAC dispersion histogram shown in gray-scale). Theoretical dispersion estimates based on the invasive-methods model (V_S profiles in Fig. 2) and inverted MAP model shown by blue and cyan lines, respectively, for each station.

IDIEM–DIC. Arrays were generally set up by the two-person UBC–EERF field crew immediately beside or surrounding the drilled borehole at each station (Fig. 3), maximizing the available open space to resolve subsurface structure to at least 30 m depth.

3.2.1. Extraction of dispersion data

For each station, the simultaneous microtremor vertical-component recordings from each array setup are processed using modified spatial autocorrelation (MSPAC) and high-resolution frequency wavenumber (HRFK) methods using Geopsy software (version 2.9.0). Dispersion estimates, fundamental-mode Rayleigh wave phase velocities at select frequencies, are retrieved primarily from the MSPAC results based on the symmetry of the array layouts; HRFK results are used primarily as a check of the MSPAC data's redundancy and therefore reliability. Each array setup provides a frequency-bandwidth limited "snapshot" of the full dispersion characteristics at each station. If the frequency-bandwidth of reliable phase velocity estimates overlaps between the array set-ups, then the mean phase velocity is calculated. Retrieval of the final dispersion curve for each station location is generally accomplished here within 1–2 days; care and expertize are required to interpret the reliable frequency bandwidth and fundamental mode of Rayleigh wave dispersion estimates.

The final retrieved dispersion estimates for 9 of the 11 investigated strong-motion stations are shown in Fig. 4, spanning frequencies of 3.8–30 Hz or a minimum and maximum depth resolution of ~4–80 m, respectively (Table 3). Amongst the 11 investigated stations, the frequency bandwidth of the retrieved dispersion data is highly variable, despite the same general field procedure, due to site-specific variables such as varying geological conditions and wavefield composition. The low-frequency limit of the non-invasive dispersion data corresponds to Rayleigh wavelengths comparable to, or greater than, the depth of the drilled boreholes. At two locations, Constucion and CCSP, a significant gap occurs at mid-frequency between retrieved dispersion estimates of the two arrays, i.e., a mid-sized ~10-m spaced array might have provided dispersion estimates linking the two segments. Overall, dispersion data accuracy would generally improve by addition of passive-source (microtremor) array
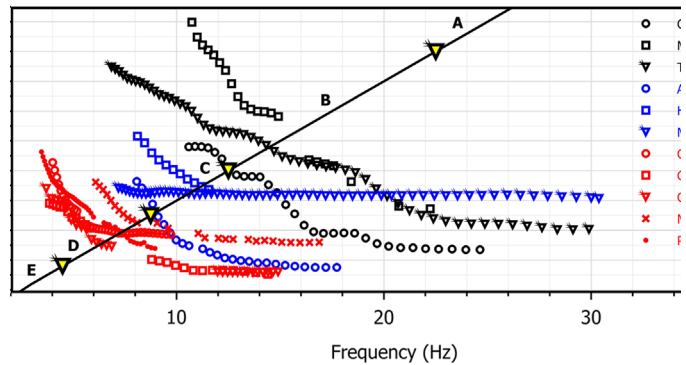
Fig. 5. Final dispersion data determined for 11 investigated stations compared with theoretical Rayleigh 40-m wavelength dispersion estimates (solid line) and associating V_{S30} site classification (labels A–E). For Melipilla and CCSP, interpolated site class estimate is provided in brackets.

sensors and array setups, as well as combination with active-source surface wave methods (e.g., MASW testing).

The measured dispersion estimates in Fig. 4 are compared with theoretical dispersion curves calculated using a 1D geophysical model based on the mean invasive-methods V_S measurements at each station. The mean invasive-methods V_S profile (Fig. 2) is converted into a 1D model: density is fixed to 2.0 g/cm^3, and V_P values are averaged from the discrete downhole V_P measurements [26]. For Melipilla and Curico, downhole V_P measurements are not available and set here to $2V_S$. The measured dispersion data and the invasive-methods dispersion estimates overlap over relatively narrow frequency (depth) intervals, and agree poorly in two cases (Constucion and CCSP). Agreement between measured and predicted dispersion estimates occurs at mid-frequencies for Casablanca, Melipilla, and Talca. At low frequencies, the retrieved dispersion data is generally higher than the predicted downhole dispersion curve indicative of higher-velocity material at depths greater than the drilled borehole.

Studies have shown high correlation between Rayleigh phase velocities at wavelengths of 35–40 m and V_{S30} [46,47]. The comprehensive relationship of [47] is: $V_{R40}=1.045V_{S30}$, where V_{R40} is

Rayleigh wave velocity at 40-m wavelength. Fig. 5 compares the final dispersion data retrieved at the 11 Chilean strong-motion stations with the theoretical dispersion estimates of a 40-m wavelength Rayleigh wave. The corresponding V_{R40} values of the measured Rayleigh dispersion data are extracted and adjusted by the relationship of [47] to estimate V_{S30} at each station and listed in Table 5. Kataoka [42] determine similar V_{S30} estimates based on dispersion V_{R40} at six stations. Fig. 5 readily demonstrates success of the non-invasive microtremor array testing campaign to retrieve V_{S30} estimates. Dispersion data, unique to each station, is retrieved spanning the intended 30-m depth (wavelength) of interest in all 11 cases for the same general field procedure.

3.2.2. Inversion methodology

Inversion of surface wave dispersion data is a non-linear and non-unique problem; the dispersion data will be adequately fit by a variety of earth model parameterizations (layering) as well as by many models (parameter combinations) for each given parameterization. Meaningful confidence intervals of model parameters are therefore required. The model parameterizations used here consist of two layers over an elastic half-space, in which all layers are characterized by uniform gradients of four elastic parameters: thickness (h), V_P, V_S, and density; V_P is related to V_S by Poisson's ratio. Linear and powerlaw gradient parameterizations are not considered here due to the intended purpose of comparison with the UCH–IDIEM–DIC mean invasive-methods i_S profile. All parameters that compose the layered model (including layer thicknesses) are free parameters, and are sampled within wide bounded uniform prior distributions.

The final dispersion curve for each station is inverted using a probabilistic (Bayesian) approach [7] which represents the solution to the inverse problem in terms of a posterior probability density (PPD) of geophysical model parameters, considered as random variables constrained by data and prior information. As this is a blind case study, all prior distributions are set to wide, yet realistic, values; hence, inversion of the frequency-limited
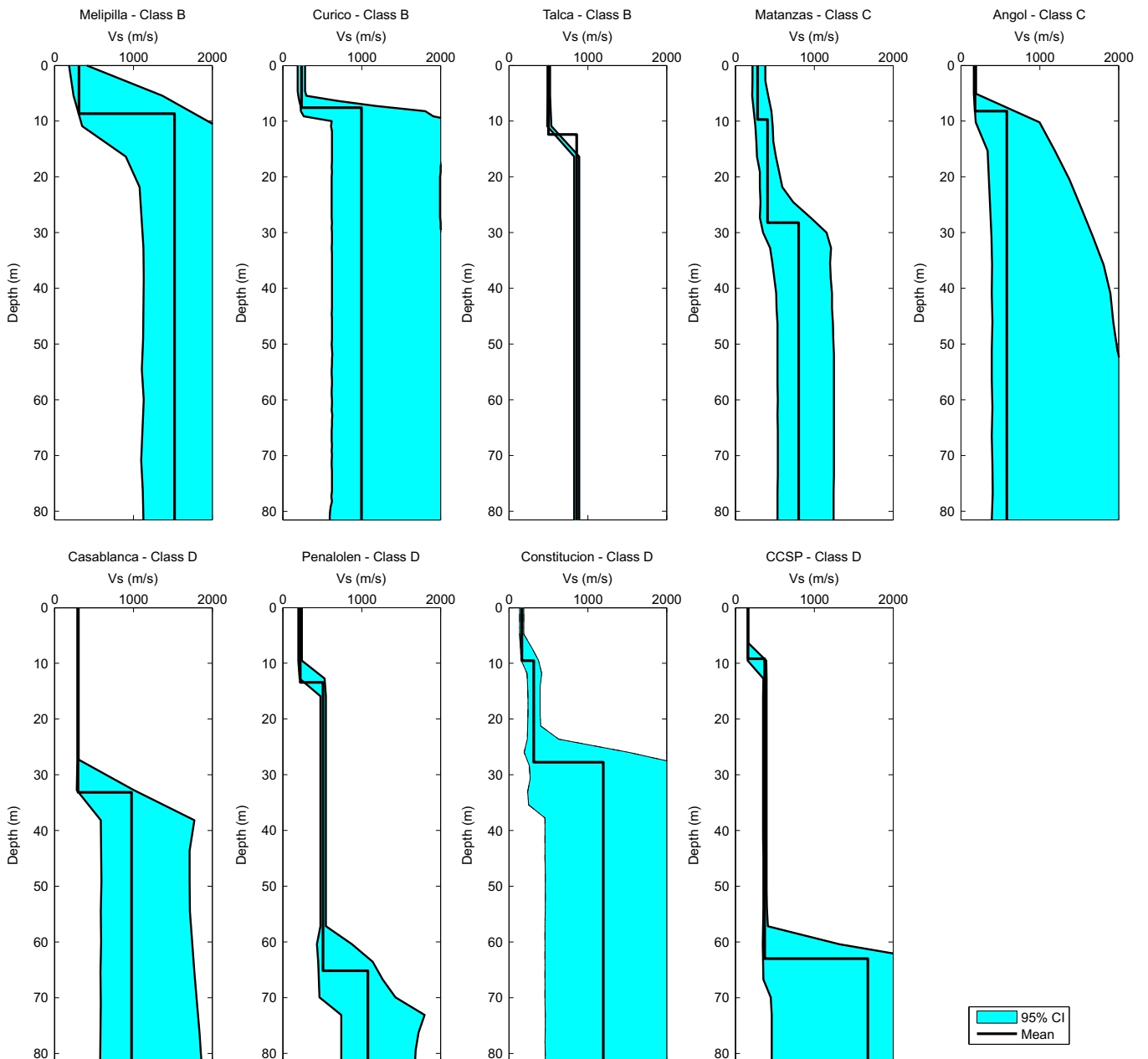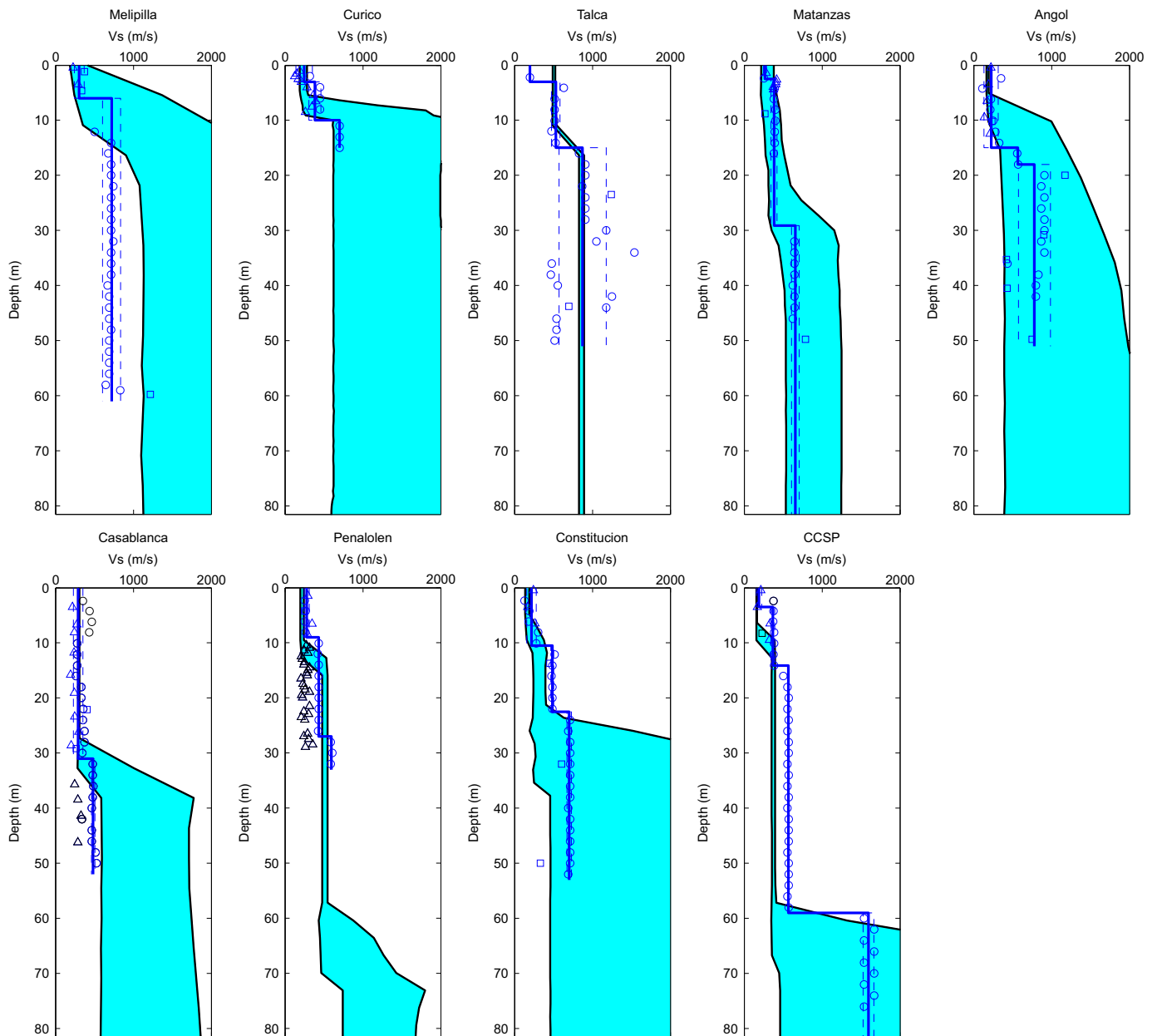

Fig. 6. For 9 investigated stations, mean V_S profile (solid line) and 95% highest probability density credibility interval (shaded area) from Bayesian inversion.

Fig. 7. For 9 investigated stations, inversion results (see Fig. 6) shown by shaded area are compared with the mean invasive-methods V_S profile (see Fig. 2) and one standard deviation estimates shown by solid and dashed lines, respectively. Invasive V_S data not included in averaging are shown by black symbols.

dispersion data will provide 1D geophysical models constrained at depths specific to the frequency (wavelength) content of the dispersion data. Stratigraphic horizons known from UCH–IDIEM–DIC borehole drilling will only be resolved by the dispersion data if the horizon coincides with a significant geophysical (impedance) contrast at depths related to the frequencies of the measured dispersion data. Computing the mean or credibility interval of selected model parameters, such as V_S and h to convert to V_S profiles, requires integrating the PPD which must be carried out numerically for nonlinear problems. Markov-chain Monte Carlo methods are used to provide an unbiased sample [7] of up to 100,000 models from the PPD here. The probabilistic inversion process is generally accomplished within a few hours per station. Agreement between the measured dispersion data and the theoretical dispersion estimates calculated for the maximum a posteriori (MAP) inversion model are shown in Fig. 4. The dispersion estimates for Hualane are limited over a very short frequency bandwidth and are very uniform for Maipu (Fig. 5), such that

inversion is not performed for these two locations. Only V_{S30} estimated from the measured V_{R40} values can be used to assign site classification based on non-invasive microtremor array testing for these two stations (Table 5).

3.2.3. Inversion results

Fig. 6 presents the mean V_S profile and 95% highest probability density (HPD) V_S profile credibility interval determined from Bayesian inversion for each station. Each model in the large PPD sample is binned onto a fine velocity-depth grid, and the 95% HPD credibility interval is computed from the probability distribution on this grid. The 95% HPD credibility interval demonstrates the quantitative uncertainty in V_S and h of each layer. For the majority of strong-motion stations, two uniform V_S layers are resolved, i.e., the elastic half-space occurs at depths greater than shown in Fig. 6. For Penalolen, Constitucion and CCSP, three distinct V_S layers are resolved, whereas at Matanzas, the 95% HPD credibility interval shows that the upper two layers are indistinguishable from each

other. For all stations, V_S is generally well resolved in the upper 30-m, which is the target depth of the field procedure and building code site classification. The maximum depth of well resolved structure is ~ 60 m (CCSP and Penalolen). Features inherent to inversion of surface wave dispersion data are apparent, such as loss of resolution with depth and lack of high-resolution (thin) layers.

Table 5 lists the V_{S30} estimate of the inverted V_S models for all stations. In general, site class B or high V_{S30} estimate stations result from a thin (≤ 10 m) low-velocity layer over a high-velocity layer, whereas site class D or low V_{S30} estimate stations result from low velocity layer(s) over the upper 30 m (Fig. 6). The two site class C or moderate V_{S30} estimate stations bound these two end member V_S profile types: a thin low velocity layer over a moderate velocity layer (Angol) or moderate velocity over the entire upper 30 m (Matanzas). Quantitative uncertainty estimates of V_{S30} provided from the probabilistic inversion are listed in Table 5: standard deviation of V_{S30} and probability of associating V_{S30} site class. Overall, quantitative uncertainty of the subsurface stiffness structure is useful for earthquake site classification according to the building code (V_{S30}) as retrieved from probabilistic inversion of non-invasive dispersion data.

4. Comparison of invasive and non-invasive V_S profiling results

Accuracy of the non-invasive microtremor-derived V_S probability distribution is assessed here by comparison with invasive UCH–IDIEM–DIC geotechnical data in terms of the average relative difference in V_S over particular depth intervals, including V_{S30} estimates and associating site class. The mean and one standard deviation of the invasive V_S datasets (downhole, laboratory BE, and converted SPT) is calculated for comparison with the non-invasive probabilistic inversion results shown in Fig. 6. As a first step, the depth partitioning of the mean invasive V_S profile is set to the same depth partitioning of the mean inverted V_S profile, which is then adjusted to the nearest layer-contrast suggested by the invasive-methods V_S data and/or stratigraphic layering. The aim is to compare not only V_S, but also layering (h), determined by the invasive and non-invasive V_S-profiling techniques. The mean invasive-methods V_S profile for each station is converted to a 1D geophysical model for calculation of theoretical dispersion estimates (as described in Section 3.2.1), and compared to the measured dispersion data in Fig. 4. Fig. 4 highlights the uniqueness of the invasive V_S measurements and non-invasive dispersion testing, providing further validation that earth model parameterization based on stratigraphic layering determined by invasive testing should not be imposed on the dispersion data during inversion for applicable earth models.

Fig. 7 shows comparison of the mean invasive V_S profile with the V_S probability distribution determined from probabilistic inversion for each station. Table 6 provides the average relative difference in V_S between the mean invasive and non-invasive V_S profiles over particular depth intervals (layers). Excellent to very good agreement is determined between the mean invasive and inverted V_S profiles over the entire 50-m borehole length for three locations: Talca, Matanzas, and Angol. For Talca, excellent agreement is obtained between the mean invasive and inverted V_S profiles to 50-m depth, with an average relative difference in V_S of 3% (Table 6). Although more complex geology and/or layering exists at Talca, the increase in V_S at ~ 15 m depth is the dominant feature of the invasive V_S and non-invasive dispersion datasets. Both invasive and non-invasive V_S profiling determines a high V_{S30} estimate corresponding to site class B. For both Matanzas and Angol, the mean invasive V_S profile occurs entirely within the 95% HPD credibility interval (Fig. 7). For Matanzas, the significant

Table 6
Average relative difference in V_S between mean invasive-methods V_S profile (interpreted) and mean inverted model.

Station	Layer depth	Average relative difference		Overall average	
	(m)	(m/s)	(%)	(m/s)	(%)
Talca	3	N/A	N/A	21	3
	15	26.0	5.0		
	> 15	15.2	1.8		
CCSP	4.5	29.9	17.0	40	8
	15	3.6	1.0		
	25.5	N/A	N/A		
	> 66.1	86.4	5.3		
Matanzas	2.5	13.7	5.0	63	11
	29	27.4	6.9		
	> 29	147.2	20.2		
Angol	15	45.0	22.3	95	19
	18	19.5	3.4		
	> 18	221.0	31.8		
Curico	3	6.5	2.7	152	19
	10	N/A	N/A		
	> 10	297.7	35.0		
Penalolen	9	57.3	23.0	69	19
	27	79.5	16.8		
	> 27	82.4	14.9		
Casablanca	31	8.8	3.0	251	35
	> 31	493.2	67.6		
Melipilla	6	4.8	1.6	405	37
	> 6	804.3	71.7		
Constitucion	10.5	55.6	29.1	239	41
	22.5	169.7	42.4		
	> 22.5	492.6	51.9		

increase in V_S at 27-m depth shown by invasive and inverted V_S profiling coincides with a stratigraphic change from normally-consolidated silts to cemented-compacted sand. For Angol, the discrete invasive V_S data exhibit greater variability than the inverted V_S profile distribution, generally coincident with stratigraphic variations. The probabilistic inversion captures uncertainty of the inverted V_{S30} estimate, 76% and 62% probability of site class C for Matanzas and Angol, respectively (Table 5). Hence, there is a higher probability that the mean invasive V_{S30} estimate is similar for Matanzas (class C) than Angol (class D), which is the case.

Excellent agreement between the mean invasive profile and non-invasive V_S probability distribution is obtained for Casablanca, Curico, and Melipilla in terms of the average relative difference in V_S ($< 3\%$; Table 6) and thickness of the uppermost layer; however, V_S at depth is significantly overestimated (Fig. 7). Overestimation of V_S at < 30 m (Melipilla) results in significantly higher non-invasive V_{S30} estimates than the mean invasive V_{S30} estimate, whereas V_S overestimation at > 30 m (Casablanca) does not result in significantly different invasive and non-invasive V_{S30} estimates. For Curico, the inversion resolves the middle of three distinct stratigraphic layers as a zone of varying V_S. However, site classification based on V_{S30} of the invasive and non-invasive V_S profiles is uniform (Table 5) at all three stations due to the excellent agreement in the V_S and depth of the uppermost low-velocity layer in all three cases.

For Constitucion and CCSP, V_S of the uppermost layer (< 10-m) is resolved in good agreement with invasive V_S measurements (Fig. 7). However, at mid-borehole depth, V_S is either underestimated (Constitucion) or not resolved (CCSP) in comparison to the invasive V_S measurements due to gaps in the mid-frequency dispersion data (Fig. 3). The reader is reminded that a two-layer model parameterization is pre-selected for all inversions; hence, it is impossible for the inversion to resolve three distinct layers for

CCSP as exhibited by the invasive V_S and stratigraphic data. The inversion determines lower V_S in the upper 30 m than measured by the invasive methods for these two stations, and therefore lower V_{S30} estimates (Table 5). For Penalolen, there is a consistent 15–20% difference in V_S of the inverted V_S probability distribution and the invasive V_S measurements over the full 35 m borehole depth (Table 6). Downhole V_S measurements show an increase in V_S at ~10-m depth although clay comprises the upper 24 m of the borehole. Converted SPT blow counts for clay material result in similar V_S values as the downhole measurements in the upper 10-m; SPT-to-V_S conversions for clay material below 10-m depth are systematically lower than downhole V_S values and are not included in the invasive-methods V_S averaging. Downhole V_S values increase again at ~24-m depth, coincident with the presence of gravels, whereas the dispersion data resolves an increase in V_S at an average depth of 65 m. Rather, the inverted dispersion data resolves V_S of a middle layer that best agrees with the average downhole V_S of the lower clay and gravel layers spanning from 10 to 32 m depth. Since the inverted models resolve a lower V_S upper layer, the resulting V_{S30} estimates are lower than invasive methods and correspond to site class D rather than C (Table 5).

5. Site classification based on predominant period

For the 11 Chilean strong-motion stations, both earthquake and microtremor recordings provide additional and unique datasets to evaluate site classification based on predominant period of the average H/V spectral ratio (Table 2). Period-based site classifications are then compared with the V_{S30}-based site classifications derived earlier from invasive and non-invasive V_S profiling. Site period is a measure of the site resonance (transfer function), related to bedrock depth, whereas V_{S30} is an average property of the upper 30 m only. Hence, site classification based on V_{S30} and site period for any given site may not fully correspond.

Available earthquake recordings include the 2010 M_W 8.8 Maule subduction event at all 11 Chilean strong-motion stations, and the 1985 M_S 7.8 Valparaiso subduction event at 4 stations. At Curico, three events are recorded: the M_W 8.8 event, and M_W 6.4 and M 6.6 events in 2004 and 2010, respectively. For all earthquake recordings, the peak ground acceleration (PGA) is > 0.1 g (Table 3) corresponding to strong ground motion and potential triggering of non-linear response of susceptible soils. Earthquake recordings obtained from UCH are bandpass-butterworth filtered. The time segment of the strongest shaking is used to compute each Fourier spectrum; time segments of 45–60 s and 30-s are used for the M_W 8.8 and M_S 7.8 events, respectively, with a 5% taper applied. The earthquake H/V spectral ratio is calculated from the smoothed average (geometric mean) horizontal spectra divided by the smoothed vertical spectrum. Fig. 8 shows the 2010 M_W 8.8 earthquake H/V spectral ratio for four selected stations calculated using Fourier velocity spectra in comparison to 5%-damped acceleration or velocity response spectra. The site classification criterion is based solely on site period; the amplification ordinate of the response spectral ratio is reduced slightly compared to the Fourier spectral ratio due to the applied 5% damping. Site period is obtainable from the spectral ratio from either acceleration or velocity recordings; traditionally, strong-motion earthquake acceleration recordings and/or microtremor velocity recordings.

The non-invasive microtremor velocity recordings conducted closest to each borehole are bandpass-butterworth filtered and cut into multiple 60-s time segments from the full ~30 min duration recording, and the average Fourier H/V spectral ratio is calculated for each time segment. The average and one standard deviation Fourier H/V spectral ratio is then calculated for all time segments. It is important to note that earthquake and microtremor recordings at the 11 Chilean strong-motion stations do not correspond to the same location; earthquake shaking is recorded by the strong-motion instrument housed within a structure at the site, whereas free-field microtremor recordings are conducted beside the drilled
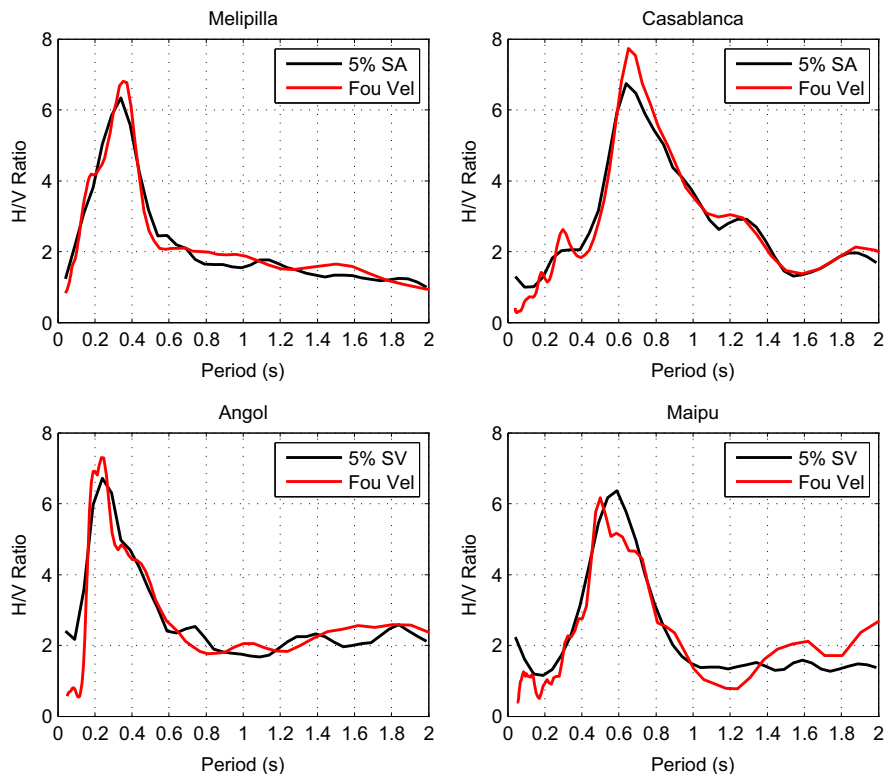

Fig. 8. Average H/V spectral ratios calculated from 2010 M_W 8.8 earthquake recordings at 4 selected stations: 5%-damped response spectral acceleration (5% SA), 5%-damped response spectral velocity (5% SV), and Fourier velocity (Fou Vel).
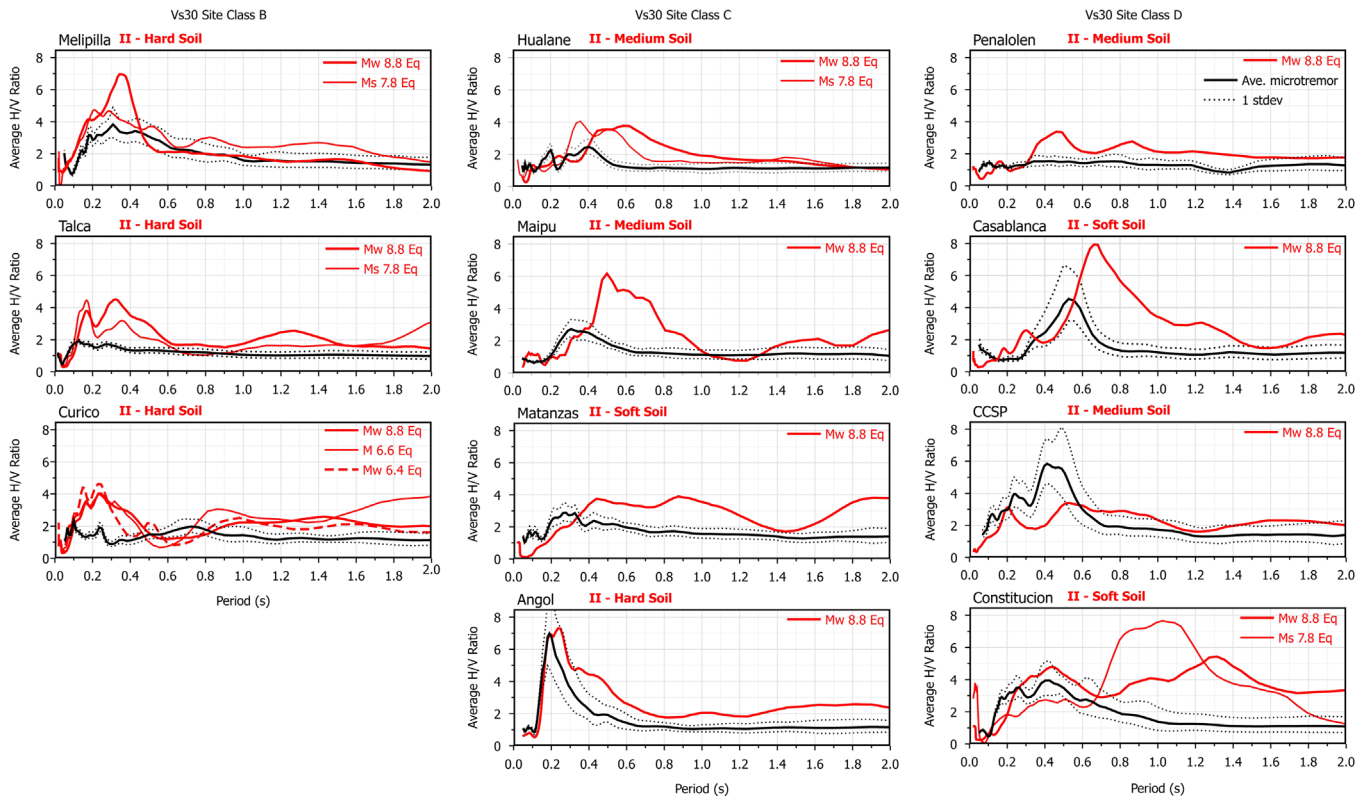
Fig. 9. Average Fourier velocity H/V spectral ratios calculated from earthquake and microtremor recordings for 11 investigated stations. Stations organized by V_{S30} site classification.

Table 7
Comparison of V_{S30}-based and period-based site classification at Chilean strong-motion stations.

Station	V_{S30} (m/s)	Site class[a] (V_{S30})	Eq.site period (s)[b]	Site class[c] (period)	Mt. site period (s)	Eq. site period [13] (s)	Site class[c] (period)
MELP – Melipilla	750	B – Soft rock or very dense soil	0.28, 0.36	II-Hard soil	0.33	0.30 0.20–0.35	II
TAL – Talca	677	B – Soft rock or very dense soil	0.33, 0.36	II-Hard soil	Flat		
CUR – Curico	554	B – Soft rock or very dense soil	0.23, 0.24, 0.24	II-Hard soil	Flat		
HUA – Hualane	460	C – Dense or firm soils	0.53, 0.59	III -Medium soil	0.40	0.38 ~0.36	II
CRS – Santiago Maipu	439	C – Dense or firm soils	0.50	III-Medium soil	0.31		
MAT – Matanzas	374	C-Dense or firm soils	0.91	IV- Soft soil	0.28		
ANGO – Angol	372	C – Dense or firm soils	0.25	II-Hard soil	0.19		
HSOR-Santiago Penalolen	330	D-Medium Firm Soils	0.45	III-Medium soil	Flat		
CSCH – Casablanca	306	D-Medium dense or firm soils	0.67	IV- Soft soil	0.53		
CCSP – Concepcion	271	D-Medium dense or firm soils	0.53	III-Medium soil	0.42		
CON – Constitucion	264	D-Medium dense or firm soils	1.02, 1.32	IV- Soft soil	0.42	0.83 ~0.74	IV

[a] Defined in Table 1.
[b] Shown in Fig. 9.
[c] Defined in Table 2.

borehole. The dimensions of each station site are generally within a city block (~0.01 km²).

Fig. 9 shows each earthquake and average microtremor Fourier H/V velocity spectral ratios for all 11 Chilean strong-motion stations. For all stations, earthquake H/V ratios demonstrate amplification at one or more periods. For stations with multiple earthquake recordings, earthquake ratios are relatively consistent between events. The average microtremor H/V ratio for the 11 stations displays either a clear site period or is rather flat, indicative of stations dominated by soft/fine-grained and stiff/coarse-grained sediments, respectively, as observed at other sites in Chile [29,33,43,44]. For Melipilla and Hualane, the earthquake and microtremor H/V ratios

observed in this study are similar to Leyton et al. [38]. Flat microtremor H/V ratios are considered agreement with short earthquake site periods (Talca and Curico). At the majority of stations, the microtremor site period is slightly shorter, and of lower amplification, than the earthquake site period. Two potential and indistinguishable factors are: (1) the earthquake motion (≥ 0.1 g) is significantly greater than microtremor motion and could potentially trigger nonlinear soil behavior and/or longer site periods at fine-grained soil sites, and (2) the depth and strength of impedance (V_S and density) contrasts in the subsurface are known to affect the ability of microtremor ratios to mimic earthquake ratios [17,29]. For example, microtremor and earthquake H/V ratios are most similar

at stations with near-surface strong impedance contrasts (Melipilla and Angol). At Constitucion, strong earthquake shaking may excite very long site periods related to longer wavelength (3D basin and/or topographic) effects.

Site classifications based on observed predominant earthquake period (Table 2) for the Chilean stations are listed in Table 7. Stations are presented in order of decreasing V_{S30} estimate determined from non-invasive microtremor V_S profiling. Stations with high V_{S30} values generally exhibit a short predominant period (<0.4 s) whereas stations with low V_{S30} values exhibit a longer predominant period (≥ 0.4 s), as expected. The stiffest coarse-grained V_{S30}-based site class B stations (Melipilla, Talca, Curico) are readily distinguished by earthquake and microtremor H/V ratios; short site periods and/or flat microtremor ratios. For all other softer site class C and D stations, observed site period is more variable. The stiffest site class C stations (Hualane and Maipu) exhibit consistent site class III medium soil site periods whereas softer site class C stations (Matanzas and Angol) display soft (site class IV) and hard (site class II) soil periods, respectively. The site class D stations display both medium and soft soil periods. The expected general trend of increasing site period with decreasing V_{S30} is observed at central and southern Chilean strong-motion stations.

6. Summary and conclusions

Inversion of non-invasive microtremor-derived dispersion data for 1D geophysical structure is accomplished in this study without knowledge of the invasive V_S profiling results, i.e. a true blind-prediction experiment. The resulting V_S profiles from discrete invasive (downhole, SPT, and laboratory BE) V_S measurements and inverted non-invasive dispersion data are compared in terms of the average relative difference in V_S, as well as V_{S30}, the main site classification criterion in the current Chilean building code.

Site conditions at the 11 strong-motion stations in central and southern Chile can be sub-divided into two major groups based on invasive V_S measurements and stratigraphy. Stations with coarse-grained gravel within the upper 10-m correspond to classes B or C: Curico, Hualane, Maipu, Melipilla, and Talca. All other stations are comprised of finer-grained sands and clays corresponding primarily to class D. Non-invasive surface wave dispersion data also demonstrate first-level approximations of site conditions at the 11 strong-motion stations. V_{S30} estimates based on the measured 40-m wavelength Rayleigh phase velocity generally correspond to the same site classifications as the invasive testing, i.e. very stiff class B–C sites are readily distinguishable from softer class C–D sites. For the majority of stations, the resulting site classification is consistent irrespective of methodology. Exceptions include Penalolen, CCSP, and Angol, in which V_{S30} estimates derived from non-invasive testing in this study correspond to lower (Penalolen and CCSP) and higher (Angol) site classifications compared to invasive methods. Overall, the non-invasive microtremor-acquired dispersion data collection, optimized for efficiency and low-cost, is able to provide a reliable assessment of V_{S30} in comparison to invasive methods for a wide variety of geological settings.

Probabilistic inversion of the non-invasive dispersion data is performed to provide uncertainty estimates of the retrieved sub-surface V_S structure. Inversion of non-invasive dispersion data is able to resolve near-surface V_S structure with generally small uncertainty, such that reasonable agreement with invasive V_{S30} estimates is obtained. The non-invasive method is able to also resolve V_S structure to similar or greater depths as invasive drilling, albeit with greater uncertainty. The overall average relative difference in V_S between mean invasive and non-invasive V_S profiles is a remarkable $\sim 10\%$ for upper soil layers and $\sim 30\%$ for the

base elastic half-space (bedrock) layer, regardless of soil conditions and/or V_{S30} site class. The assumption to be made here is that non-invasive V_S profiling performed at any other location in central and southern Chile will provide V_S measurements within $\sim 20\%$ of invasive V_S measurements, on average. This blind-comparison study has demonstrated that efficient and low-cost non-invasive microtremor array testing is a credible V_S profiling technique in a wide variety of geological conditions and may be used in the future with confidence throughout Chile and elsewhere.

Empirical earthquake and microtremor H/V spectral ratios are calculated to evaluate predominant site period as an additional and/or independent site classification criterion. The expected general trend of short site periods related to stiff soils (high V_{S30}) and longer site periods related to medium to soft soils (low V_{S30}) is observed. However, earthquake site response classification based on site period is more sensitive to the underlying V_S structure than V_{S30}. For example, V_{S30} estimates determined for Matanzas and Angol stations correspond to site class C dense or firm soil conditions, but the different underlying V_S structure at these two stations results in different site periods: very consistent and short period (hard soil) behaviour at Angol results from low velocity fine-grained clays and sands to ~ 14 m depth over high velocity volcanic tuff, whereas longer period (medium soil) behaviour at Matanzas results from moderate velocity fine-grained clays and sands to more than 50 m depth. The use of site period in combination with V_{S30} ensures robust earthquake site response prediction.

Data and resources

Chilean earthquake data was downloaded at http://terremotos.ing.uchile.cl (last accessed December 2013) and the Strong-Motion Virtual Data Center (VDC) at http://www.strongmotioncenter.org/vdc (last accessed August 2014). Software for microtremor array data processing obtained at www.geopsy.org (last accessed December 2013). Mathworks Matlab software was used for plotting. Fig. 1 generated using GeoMapApp (www.geomapapp.org, last accessed December 2013).

References

[1] Guendelman T, Saragoni GR, Verdugo R. Chilean emergency seismic design code for building after El Maule 2010 earthquake. In: Proceedings of the Fifteenth World Conference on Earthquake Engineering, Lisbon, Portugal, Paper 4480; 2012.

[2] Stokoe KH, Wright SG, Bay JA, Roesset JM. Characterization of geotechnical sites by SASW method. In: Woods RD, editor. Geophysical characterization of sites. Proceedings of the thirteenth ICSMFE. New York: International Science Publisher; 1994. p. 15–25.

[3] Park CB, Miller RD, Xia J. Multichannel analysis of surface waves. Geophysics 1999;64:800–8.

[4] Aki K. Space and time spectra of stationary stochastic waves, with special reference to microtremors. Bull Earthq Res Inst 1957;35:415–56.

[5] Asten MW, Henstridge JD. Array estimators and use of microseisms for reconnaissance of sedimentary basins. Geophysics 1984;49:1828–37.

[6] Horike M. Inversion of phase velocity of long-period microtremors to the S-wave-velocity structure down to the basement in urbanized areas. J Phys Earth 1985;33:59–96.

[7] Molnar S, Dosso SE, Cassidy JF. Bayesian inversion of microtremor array dispersion data in southwestern British Columbia. Geophys J Int 2010;183:923–40.

[8] Xia J, Miller RD, Park CB, Hunter JA, Harris JB. Comparing shear-wave velocity profiles from MASW with borehole measurements in unconsolidated sediments, Fraser River delta, BC, Canada. J Environ Eng Geophys 2000;5:1–13.

[9] Xia J, Miller RD, Park CB, Hunter JA, Harris JB, Ivanov J. Comparing shear-wave velocity profiles inverted from multichannel surface wave with borehole measurements. Soil Dyn Earthq Eng 2002;22:181–90.

[10] Woeller DL, Luternauer JL, Hunter JA. Presentation and interpretation of seismic cone penetration test data, Fraser River delta, British Columbia. Geological Survey of Canada, Open file 2715; 1993.

[11] Molnar S, Ventura CE, Finn WDL, Taiebat M, Dosso S, Cassidy JF. Evaluation of shear-wave velocity profiles from ambient vibration array recordings in SW British Columbia, Canada. In: Proceedings of the fifteenth world conference on earthquake engineering, Lisbon, Portugal, Paper 3175, 2012.

[12] Moss RES. Quantifying measurement uncertainty of thirty-metre shear-wave velocity. Bull Seismol Soc Am 2008;98:1399–411.

[13] Arango MC, Strasser FO, Bommer JJ, Boroschek R, Comte D, Tavera H. A strong-motion database from the Peru–Chile subduction zone. J Seismol 2011;15:19–41.

[14] Verdugo R. Amplification phenomena observed in downhole array records generated on a subductive environment. Phys Earth Planet Inter 2009;175:63–77.

[15] Borcherdt RD. Effects of local geology on ground motion near San Francisco Bay. Bull Seismol Soc Am 1970;60:29–61.

[16] Lermo J, Chavez-Garcia FJ. Site effect evaluation using spectral ratios with only one station. Bull Seismol Soc Am 1993;83:1574–94.

[17] Bard P-Y. Microtremor measurements: a tool for site effect estimation? In: Proceedings of the second international symposium on the effects of surface geology on seismic motion, Yokohama, Japan; 1999. pp. 1251–79.

[18] Kawase H, Nagashima F, Matsushima S, Sanchez-Sesma FJ. Application of horizontal-to-vertical (H/V) spectral ratios for both microtremors and earthquake motions based on the diffuse field theory, In: Proceedings of the 10th US National Conference on Earthquake Engineering, Anchorage, Alaska, Paper 928; 2014.

[19] Molnar S, Cassidy JF. A comparison of site response techniques using weak-motion earthquakes and microtremors. Earthq Spectra 2006;22:169–88.

[20] Zaré M, Bard P-Y, Ghafory-Ashtiany M. Site characterizations for the Iranian strong motion network. Soil Dyn Earthq Eng 1999;18:101–23.

[21] Ghasemi H, Zare M, Fukushima Y, Sinaeian F. Applying empirical methods in site classification, using response spectral (H/V): a case study on Iranian strong motion network (ISMN). Soil Dyn Earthq Eng 2009;29:121–32.

[22] Lee C-T, Cheng C-T, Liao C-W, Tsai Y-B. Site classification of Taiwan free-field strong-motion stations. Bull Seismol Soc Am 2001;91:1283–97.

[23] Yamazaki F, Ansary MA. Horizontal-to-vertical spectrum ratio of earthquake ground motion for site characterization. Earthq Eng Struct Dyn 1997;26:671–89.

[24] Zhao JX, Zhang J, Asano A, Ohno Y, Oouchi T, Takahashi T, Ogawa H, Irikura K, Thio HK, Somerville PG, Fukushima Y, Fukushima Y. Attenuation relations of strong ground motion in Japan using site classification based on predominant period. Bull Seismol Soc Am 2006;96:898–913.

[25] Di Alessandro C, Bonilla LF, Boore DM, Rovelli A, Scotti O. Predominant-period site classification for response spectra prediction equations in Italy. Bull Seismol Soc Am 2012;102:680–95.

[26] Boroschek RL, Yáñez U. F, Bejarano B. I, Molnar S, Torres G. A. Caracterizacion geotecnica estaciones de acelerografos de la Universidad de Chile, Report of FCFM (Facultad de Ciencias Físicas y Matemáticas) and IDIEM. Santiago: Universidad de Chile; 2012. p. 587.

[27] Moreno T, Gibbons W, editors. The geology of Chile. London: The Geological Society; 2007.

[28] Taylor GC. Geology and ground water of the Casablanca basin, Chile. Econ Geol 1948;43:661–74.

[29] Bonnefoy-Claudet S, Baize S, Bonilla LF, Berge-Thierry C, Pasten C, Campos J, Volant P, Verdugo R. Site effect evaluation in the basin of Santiago de Chile using ambient noise measurements. Geophys J Int 2009;176:925–37.

[30] Bonnefoy-Claudet S, Leyton F, Baize S, Berge-Thierry C, Bonilla LF, Campos J, Potentiality of microtremor to evaluate site effects at shallow depths in the deep basin of Santiago de Chile. In: Proceedings of the fourteenth world conference on earthquake engineering, Beijing, China; 2008.

[31] Assimaki D, Ledezma C, Montalva GA, Tassara A, Mylonakis G, Boroschek R. Site effects and damage patterns. Earthq Spectra 2012;28:S55–74.

[32] Araneda M, Monge J, Avendano MS. Microzoning studies in the Maule region, Chile. In: Proceedings of the eleventh world conference on earthquake engineering, Acapulco, Mexico, Paper 702; 1996.

[33] Leyton F, Ruiz S, Sepúlveda SA, Contreras JP, Rebolledo S, Astroza M. Microtremors' HVSR and its correlation with surface geology and damage observed after the 2010 Maule earthquake (M_W 8.8) at Talca and Curicó, Central Chile. Eng Geol 2013;161:26–33.

[34] Villalobos F, Ovando E, Mendoza M, Oróstegui P. Damages observed in the 2010 Concepción earthquake related to soil phenomena. In: Proceedings of the fifth international conference on earthquake geotechnical engineering, Santiago, Chile, Paper DOCV; 2011.

[35] Toshinawa T. Matsuoka M, Yamazaki Y. Ground-motion characteristics in Santiago, Chile, obtained by microtremor observations. In: Proceedings of the eleventh world conference on earthquake engineering, Acapulco, Mexico, Paper 1764; 1996.

[36] Cruz EF, Riddell R, Fernandez L, Valdivia D. A study of site amplification effects in Santiago based on earthquake records obtained from the SMASCH array. In: Proceedings of the 12th world conference on earthquake engineering, Auckland, New Zealand; 2000.

[37] Verdugo R, Pasten C. Observation of seismic amplification on subductive environment. In: Proceedings of the fourth international conference on earthquake geotechnical engineering, Thessaloniki, Greece, Paper 1462; 2007.

[38] Leyton F, Ruiz S. Comparison of the behaviour of site from strong motion data of 1985 Central Chile earthquake (MW 7.8) and microtremor measurements. In: Proceedingsm of the fifth international conference on earthquake geotechnical engineering, Santiago, Chile, Paper CBSLR; 2011.

[39] Pilz M, Parolai S, Leyton F, Campos J, Zschau J. A comparison of site response techniques using earthquake data and ambient seismic noise analysis in the large urban areas of Santiago de Chile. Geophys J Int 2009;178:713–28.

[40] Ramirez P, Vivallos J. Microzonificación sísmica de la ciudad de Concepción-Chile. In: Proceedings of the XII Congreso Geológico Chileno, Santiago, Chile, S3_018, 2009.

[41] Midorikawa S. Site effects on strong-motion records of the 1985 Chile earthquake and their nonlinear behaviour. In: Proceedings of the tenth world conference on earthquake engineering, Madrid, Spain; 1992.

[42] Kataoka S. Microtremor exploration at seven strong-motion stations in Chile. In: Proceedings of the fourth IASPEI/IAEE international symposium, effects of surface geology on seismic motion, University of California Santa Barbara; 2011.

[43] Sekiguchi T, Pulido N, Shoji G, Alba J, Lazares F. Strong ground motions and site effects of the 2010 Chile earthquake. In: Proceedings of the eighth international conference on urban earthquake engineering, Tokyo, Japan; 2011.

[44] Leyton F, Montalva G, Ramirez P. Towards a seismic microzonation of Concepción urban area based on microtremors, surface geology, and damage observed after the Maule 2010 earthquake, First Results. In: Proceedings of the fourth IASPEI/IAEE international symposium, effects of surface geology on seismic motion, University of California Santa Barbara; 2011.

[46] Konno K, Kataoka S. New method for estimating the average s-wave velocity of the ground. In: Proceedings of the Sixth International Conference on Seismic Zonation, Palm Springs, California; 2000.

[47] Brown LT, Diehl JG, Nigbor RL. A simplified procedure to measure average shearwave velocity to a depth of 30 m (VS30). In: Proceedings of the sixth international conference on seismic zonation, Palm Springs, California; 2000.

[48] Barrientos S. Terremoto Cauquenes 27 Febrero 2010. Informe tecnico actualizado 27 Mayo 2010, Servicio Seismologico, Universidad de Chile; 2010. 20p.

[49] Wood SL, Wight JK, Moehle JP. The 1985 Chile earthquake: observations on earthquake-resistant construction in Viña del Mar. Civil Engineering Studies. Structural research series No. 532, University of Illinois at Urbana-Champaign, Urbana, Illinois; 1987. 186 p.

[50] Brandenburg, SJ, Ballana N, Shantz T. Shear wave velocity as a statistical function of standard penetration test resistance and vertical effective stress at Caltrans Bridge Sites, Pacific Earthquake Engineering Research Center, College of Engineering, PEER Report 2010/03, University of California, Berkeley, California; 2010.